agriculture

MDPI

Article

Unmanned-Aerial-Vehicle-Based Multispectral Monitoring of Nitrogen Content in Canopy Leaves of Processed Tomatoes

Hao Zhang [1,2], Li Zhang [1,2], Hongqi Wu [1,2,*], Dejun Wang [3], Xin Ma [1,2], Yuqing Shao [1], Mingjun Jiang [1,2] and Xinyu Chen [1,2]

[1] College of Resources and Environment, Xinjiang Agricultural University, Urumqi 830052, China; 320223643@xjau.edu.cn (H.Z.); zhangli0628@xjau.edu.cn (L.Z.); 320243739@stu.xjau.edu.cn (X.M.); 320223628@stu.xjau.edu.cn (Y.S.); 320212561@xjau.edu.cn (M.J.); 320233703@xjau.edu.cn (X.C.)
[2] Xinjiang Engineering Technology Research Center of Soil Big Data, Urumqi 830052, China
[3] Institute of Western Agriculture, CAAS, Changji 831100, China; wangdejun@caas.cn
* Correspondence: whq@xjau.edu.cn; Tel.: +86-139-9925-1674

Abstract: Nitrogen serves as a critical nutrient influencing the yield and quality of processed tomatoes; however, traditional methods for assessing its levels are both labor-intensive and costly. This study aimed to explore an efficient monitoring approach by analyzing the relationship between leaf nitrogen content (LNC) and canopy spectral reflectance characteristics throughout the growth stages of processed tomatoes at the Laolong River Tomato Base in Changji City, Xinjiang. The experimental design incorporated nine treatments, each with three replicates. LNC data were obtained using a dedicated leaf nitrogen content analyzer, while drones were utilized to capture multispectral images for the extraction of vegetation indices. Through Pearson correlation analysis, the optimal spectral variables were identified, and the relationships between LNC and spectral variables were established using models based on backpropagation (BP), multiple linear regression (MLR), and random forests (RFs). The findings revealed that the manually measured LNC data exhibited two peak values, which occurred during the onset of flowering and fruit setting stages, displaying a bimodal pattern. Among the twelve selected vegetation indices, ten demonstrated spectral sensitivity, passing the highly significant 0.01 threshold, with the Normalized Difference Chlorophyll Index (NDCI) showing the highest correlation during the full bloom stage. The combination of the NDCI and RF model achieved a prediction accuracy exceeding 0.8 during the full bloom stage; similarly, models incorporating multiple vegetation indices, such as RF, MLR, and BP, also reached prediction accuracies exceeding 0.8. Consequently, during the seedling establishment and initial flowering stages (vegetation coverage of <60%), the RF model with multiple vegetation indices was suitable for monitoring LNC; during the full bloom stage (vegetation coverage of 60–80%), both the RF model with the NDCI and the MLR model with multiple indices proved effective; and during the fruit setting and maturation stages (vegetation coverage of >80%), the BP model was more appropriate. This research provides a scientific basis for the cultivation management of processed tomatoes and the optimization of nitrogen fertilization within precision agriculture. It advances the application of precision agriculture technologies, contributing to improved agricultural efficiency and resource utilization.

Keywords: processed tomato; leaf nitrogen content; UAV remote sensing technology; vegetation cover; vegetation index; precision agriculture

Received: 11 November 2024
Revised: 16 December 2024
Accepted: 27 January 2025
Published: 30 January 2025

Citation: Zhang, H.; Zhang, L.; Wu, H.; Wang, D.; Ma, X.; Shao, Y.; Jiang, M.; Chen, X. Unmanned-Aerial-Vehicle-Based Multispectral Monitoring of Nitrogen Content in Canopy Leaves of Processed Tomatoes. *Agriculture* **2025**, *15*, 309. https://doi.org/10.3390/agriculture15030309

1. Introduction

Tomatoes are extensively cultivated across the globe, with China's Xinjiang region emerging as one of the world's three premier zones for tomato cultivation and processing, thanks to its unique natural conditions. By 2023, the area dedicated to processing tomatoes in Xinjiang had reached 64.66 million hectares, with a total yield of 4.35 million tons, accounting for 80% of the national output. Additionally, processed tomato products from this region constitute approximately 15% of the global supply, a figure that is steadily increasing [1]. Nitrogen plays an exceedingly vital role in the growth process of processed tomatoes; insufficient nitrogen fertilization can significantly affect plant growth, fruit yield, and quality and may adversely impact plant resilience and soil health [2]. Conversely, excessive fertilization can lead to abnormal plant morphology, an imbalanced allocation of photosynthates, diminished fruit quality, and potential environmental pollution and resource wastage [3–6]. Therefore, the rapid monitoring and precise management of nitrogen distribution in processed tomato fields are of paramount importance [7]. Traditional manual monitoring methods are not only inefficient and inadequate for capturing nitrogen distribution information over large agricultural areas, but are also susceptible to human error. Consequently, there is an urgent need for an innovative monitoring approach that can deliver accurate, real-time data on crop nitrogen distribution, providing scientific and technological support for the monitoring and assessment of the leaf nitrogen content in processed tomatoes.

With the continuous advancements and innovations in UAV remote sensing technology, a plethora of cutting-edge methodologies have emerged for the rapid and non-destructive monitoring of field crop growth parameters. Numerous scholars have conducted extensive and in-depth research in this area, achieving significant breakthroughs, particularly in the monitoring of crop nitrogen content. For instance, Lee et al. [8] utilized UAV-acquired multispectral imagery to monitor the canopy nitrogen content in cornfields in southwestern Ontario, Canada. Among the models employed, the RF model demonstrated a superior performance due to its high accuracy and interpretability. This model was subsequently applied to UAV imagery captured at various growth stages to generate spatial variation maps of canopy nitrogen content, facilitating efficient monitoring. Traditional vertical collection methods often result in inaccurate estimations of leaf nitrogen content. Lu et al. [9] explored the use of multi-angle spectral data to enhance the estimation accuracy for LNC. By integrating multiple vegetation indices and developing models using a multi-angle composite vegetation index, they improved the accuracy of nitrogen content estimation in winter wheat, providing scientific guidance for nitrogen fertilizer management. Wang et al. [10] employed a leaf nitrogen content analyzer (TYS-4N) for the in vivo determination of the nitrogen content in rice leaves, finding the measurement errors to be within acceptable limits and the timeliness to be high, offering a feasible in vivo measurement method and reliable data foundation for research on rice leaf nitrogen content. Liu et al. [11], by obtaining UAV hyperspectral data in conjunction with empirical data, utilized MLR and BP models to validate the model effectiveness. They found that the predictive values for winter wheat during the jointing, flowering, and defoliation stages were ideal, thereby demonstrating the reliability and precision of UAV hyperspectral data.

The aforementioned studies primarily relied on UAV remote sensing imagery to extract characteristic parameters and establish correlations with physiological indicators of crop nitrogen content, thus enabling the determination of nitrogen levels in crops. However, existing research has yet to comprehensively cover the monitoring of LNC throughout the entire growth cycle of crops. Moreover, there remains a lack of thorough evaluation regarding the applicability of different vegetation indices for modeling and monitoring

across the full growth cycle, or the effectiveness of a single index for LNC monitoring throughout the entire growth period.

To address these gaps, this study integrates ground-based surveys with UAV remote sensing methods to systematically monitor the LNC of processed tomatoes, as illustrated in Figure 1. The objectives of this research are threefold, as follows: (1) to elucidate the dynamic variation characteristics of the LNC in processed tomatoes at different growth stages; (2) to explore the predictive performance of vegetation indices in conjunction with RF, BP, and MLR models throughout the entire growth cycle of processed tomatoes; and (3) to identify the optimal strategy for LNC monitoring during the full growth cycle of processed tomatoes under varying vegetation cover conditions, through a comparative analysis of leaf nitrogen content estimation models constructed using single variables versus multiple variables.

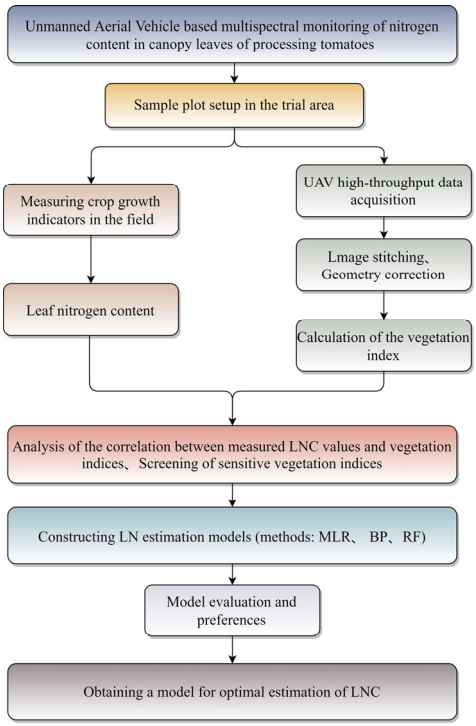

Figure 1. Theoretical framework for the study.

2. Materials and Methods

2.1. Overview of the Research Area

The study area is located in the Modern Agricultural Demonstration Park of the National Agricultural Science and Technology Park in Changji Hui Autonomous Prefecture, Xinjiang Uygur Autonomous Region, specifically in the Laolonghe area of Changji City, which is located at the northern foothill of the Tianshan Mountain at an elevation of about 490 m above sea level, as shown in Figure 2. Nestled on the northern slopes of the Tianshan Mountains, at an elevation of approximately 490 m, this region boasts a predominantly arid climate, receiving an annual precipitation of merely 190 mm. The average yearly temperature stands at 6.8 °C, with an impressive 2700 h of sunshine annually. Blessed with abundant water resources, flat terrain, and fertile soil, this area has emerged as the preeminent hub for tomato processing in Xinjiang. It commands a significant presence, with a comprehensive supply chain that encompasses the entire tomato industry. Covering 41% of the region's tomato cultivation area, it hosts 25 tomato product processing enterprises, including one recognized as a national leader. These enterprises account for 35% of the region's processing capacity, with the industry chain's value projected to exceed CNY

3 billion [12]. Thus, it is unequivocally an ideal location for conducting research on tomato processing.

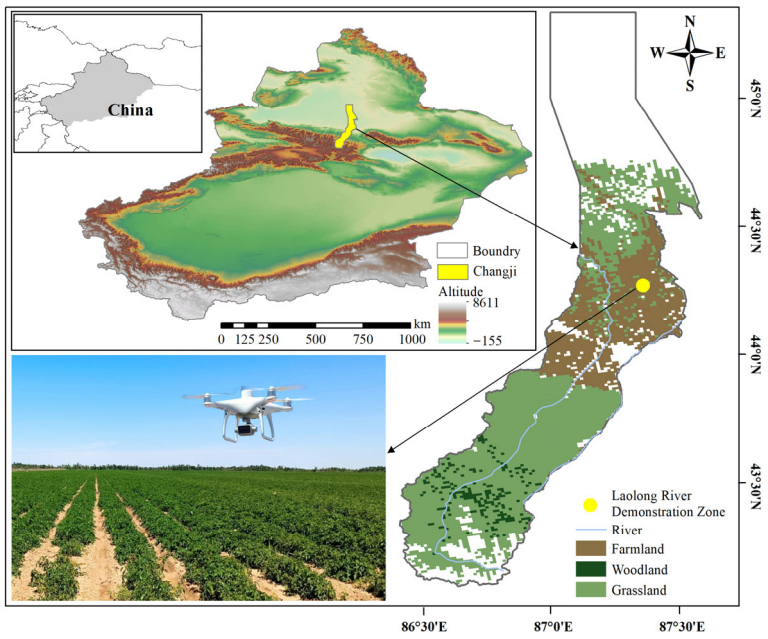

Figure 2. Geographical location of study area.

2.2. Experimental Design

In 2023, this study selected the Tunhe 1911 processing tomato variety for experimentation. The entire growth cycle commenced with transplanting on May 16 and concluded with harvesting on August 26. The cultivation methodology employed was seedling transplantation. Once the seedlings, aged from 40 to 50 days in trays, reached the growth stage of four to five true leaves, they were transplanted into the open field.

The experimental plot spanned a total width of 200 m, employing a twin-row ridge planting system. The spacing between rows on each ridge was 0.3 m, while the interval between ridges was 1.5 m, with plants spaced at 0.2 m apart and planted at a depth from 0.01 to 0.02 m. The experiment comprised nine treatments, each replicated across three ridges, with each ridge extending 760 m in length, resulting in a total of 27 individual plots. A designated area, measuring 210 m in length and 120 m in width, was earmarked as the research zone, where drone-based remote sensing and manual ground surveys were conducted concurrently.

2.3. Data Acquisition and Pre-Processing

2.3.1. UAV Multispectral Data

Throughout the entire growth period of the tomatoes, encompassing the transplant recovery phase (19 May–7 June), flowering initiation (8 June–28 June), full bloom (29 June–11 July), fruit setting (12 July–28 July), and the ripening stage (29 July–13 August), multispectral data monitoring was conducted using the DJI Phantom 4 Multispectral (Shenzhen DJI Innovation Technology Co. Ltd., Shenzhen, China). This UAV, equipped with a multispectral camera, is capable of capturing data across the following five spectral bands: blue (450 ± 16 nm), green (560 ± 16 nm), red (650 ± 16 nm), red edge (730 ± 16 nm), and near-infrared (840 ± 26 nm). The aircraft autonomously executed pre-programmed flight routes, transmitting real-time aerial imagery back to operators. Efforts were made to collect multispectral images under ideal weather conditions—clear skies, no wind—between 12:00 and 15:00, to ensure the quality and reliability of the images while optimizing flight safety and operational efficiency. The flight paths were configured with a longitudinal overlap of

80% and a lateral overlap of 70%, maintaining a flight speed of 1.7 m/s at an altitude of 25 m, achieving a resolution of 1.3 cm/px. Subsequently, the captured images were processed using Pix4Dmapper 4.5.6 (Pix4D SA, Prilly, Switzerland) software to stitch together a comprehensive multispectral image of the experimental field, as depicted in Figure 3. Further analysis, including spatial and geometric corrections, as well as vegetation index calculations, was conducted using ENVI 5.3 software.

Figure 3. UAV image stitching diagram.

2.3.2. Measurement of Leaf Nitrogen Content

Simultaneously with the acquisition of canopy multispectral data, the LNC of the tomatoes was measured using the ZKWH TYS-4N (Beijing Zhongke Weihe Technology Development Co., Beijing, China) handheld nitrogen content analyzer [13]. Before each measurement, the surface of the instrument was cleaned with a wiping cloth to remove any dirt or impurities, and calibration was performed to ensure its proper operation and accuracy. In the nine treatments, three replicate samples were taken each time, selecting 10 uniformly growing, representative processed tomato plants each time, totaling 270 plants. Depending on the leaf area size and leaf color distribution differences in the canopy leaves, from 5 to 10 points were measured per leaf, and the average value was taken. Consequently, a total of 1350 data sets were obtained to represent the nitrogen content in the leaves of processed tomatoes within the experimental area.

2.4. Data Analysis and Applications

2.4.1. Selection and Construction of Vegetation Indices

The Vegetation Index (VI) is a quantitative metric utilized to assess and monitor vegetation growth, health, and coverage through remote sensing technology. It is generated based on the spectral characteristics of vegetation, employing the ratio or linear combination of reflectance from two or more distinct spectral bands. The VI is instrumental in monitoring various vegetation characteristics, such as estimating crop physical parameters, analyzing land use and cover, and supporting climate models and ecological simulations. In this

study, informed by previous research findings and the relevant literature, we selected twelve vegetation indices closely correlated with LNC to enhance the accuracy of nitrogen content monitoring in crop leaves, as detailed in Table 1.

Table 1. Vegetation indices and their calculation formulas.

Vegetation Indices	Acronym	Expressions	References
Normalized Difference Chlorophyll Index	NDCI	(RE − R)/(RE + R)	[14]
Normalized Difference Red Edge Index	NDRE	(NIR − RE)/(NIR + RE)	[15]
Normalized Pigment Chlorophyll Index	NPCI	(R − B)/(R + B)	[16]
Ratio Vegetation Index	RVI	NIR/R	[17]
Triangular Vegetation Index	TVI	0.5(120(NIR − G) − 200(R − G))	[18]
Normalized Difference Vegetation Index	NDVI	(NIR − R)/(NIR + R)	[19]
Transformed Chlorophyll Absorption in Reflectance Index	TCARI	3[(RE − R) − 0.2(RE − G) × (RE/R)]	[20]
Visible Atmospherically Resistant Index	VARI	(G − R)/(G + R - B)	[21]
Red Edge Ratio Difference Vegetation Index	RERDVI	(NIR − RE)/ $\sqrt{(NIR + RE)}$	[22]
Soil-Adjusted Vegetation Index	SAVI	1.5(NIR − R)/(NIR + R + 0.5)	[23]
Modified Triangular Vegetation Index	MTCI	(NIR − RE)/(RE − R)	[24]
Structure Insensitive Pigment Index	SIPI	(NIR − B)/(NIR + R)	[25]

Note: blue (B), green (G), red (R), red edge (RE), and near-infrared (NIR) correspond to the reflectance at the 450 nm, 560 nm, 650 nm, 730 nm, and 840 nm spectral bands, respectively, as collected by the UAV.

2.4.2. Model Construction and Validation

A correlation analysis was conducted between the selected multispectral image variables and the measured LNC to ascertain their interrelationships and identify the spectral variables with higher correlations. Subsequently, these selected variables were modeled using the BP, MLR, and RF techniques. Across all growth stages, a total of 1350 data sets were compiled. To ensure the reliability and generalization capability of the models, 70% of the sample data was randomly selected as the training set for constructing the LNC estimation model for the processed tomatoes. The remaining 30% of the data served as an independent test set to evaluate the predictive performance of the developed models.

2.4.3. Model Accuracy Evaluation Metrics

In this study, the coefficient of determination (R^2), Root Mean Square Error (*RMSE*), and Mean Absolute Error (*MAE*) were employed as metrics to evaluate the model accuracy. The R^2 metric is utilized to assess the degree of fit between the observed values and a model's predictions [26]. *RMSE*, being sensitive to outliers, offers an overall measure of predictive error. In contrast, *MAE* provides a straightforward indication of the average error magnitude, being less influenced by outliers, and both metrics can be used to assess the deviations between observed values and model predictions [27]. Higher R^2 and lower *RMSE* and *MAE* values indicate a better goodness of fit, reflecting a superior estimation accuracy and model stability. The corresponding formulas are as follows:

$$R^2 = 1 - \frac{\sum_{i=1}^{N}(\hat{y}_i - y_i)^2}{\sum_{i=1}^{N}(y_i - \overline{y})^2} \quad (1)$$

$$RMSE = \sqrt{\frac{1}{N}\sum_{i=1}^{N}(\hat{y}_i - y_i)^2} \quad (2)$$

$$MAE = \frac{1}{N}\sum_{i=1}^{N}|\hat{y}_i - y_i| \quad (3)$$

In these formulas, $\hat{y}_i$ represents the predicted value for the i-th sample, y_i denotes the actual value for the i-th sample, $\overline{y}$ is the mean of the actual sample values, and N indicates the total number of samples.

3. Results and Analysis

3.1. Observed Dynamic Changes in LNC of Processed Tomatoes at Different Growth Stages

The trajectory of the LNC in the processed tomatoes across different growth phases is illustrated in Figure 4. During the seedling establishment stage, the median LNC was recorded at 8.74, indicative of relatively low nitrogen levels, as the crops were in the initial stages of germination and their root systems had not yet fully developed, limiting their nutrient absorption capabilities. As the plants progressed to the flowering initiation phase, the LNC markedly rose to 13.7, suggesting a significant increase in nitrogen demand, coinciding with the differentiation of flower buds and the flowering process. At this stage, the crops required substantial nitrogen to support the formation and growth of flowers. Subsequently, during the peak flowering period, the LNC value further elevated to 11.2. Although this was a slight decrease from the flowering initiation phase, it remained elevated, reflecting the nitrogen demand associated with full bloom and the pollination process. As the plants entered the fruit setting stage, their nitrogen content experienced another rise, peaking at 15.2, indicating the highest nitrogen demand during the development of the fruit. This stage necessitated considerable nitrogen to facilitate cell division and rapid growth. In the maturation phase, the leaf nitrogen content slightly declined to 12.8, reflecting relatively lower nitrogen requirements, yet it was still essential to support full fruit ripening and the accumulation of nutrients. Overall, the leaf nitrogen content in the processed tomatoes reached its zenith during the fruit setting stage, followed by a decline as the plants approached maturity.

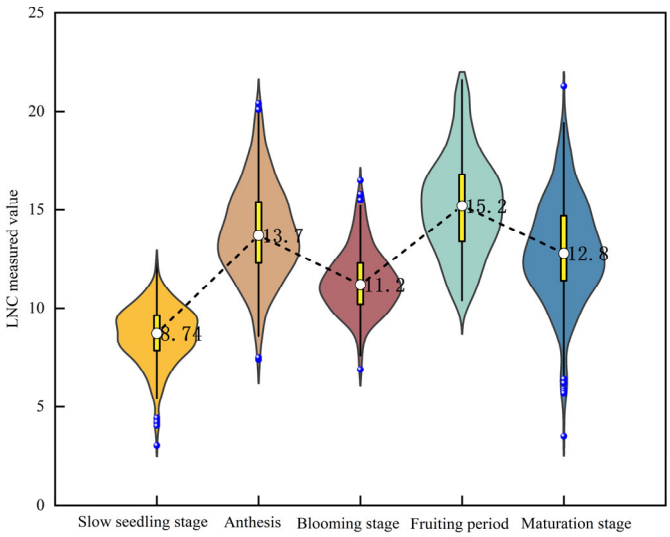

Figure 4. Plot of changes in measured processed tomato LNC over the full life span.

3.2. Correlation Analysis Between Measured LNC Values and Multispectral Vegetation Indices

A Pearson correlation analysis was performed between spectral variables and the measured LNC values of the processed tomatoes across five growth stages, as depicted in Figure 5. Among these stages, the full flowering period exhibited the highest correlation of spectral indices with LNC at the 0.01 significance level, with absolute values ranging from 0.54 to 0.76. Notably, the NDCI showed the strongest correlation at 0.75. During the flowering initiation and fruit setting stages, the NDCI also demonstrated higher correlations at the 0.01 level, with values of 0.73 and 0.70, respectively. In the seedling establishment

phase, the RVI displayed a notable correlation of 0.64 at the 0.01 level. Conversely, in the maturation phase, most spectral indices, except for the MTCI, TVI, and SAVI, reached significance levels, with the NDCI again showing the highest correlation at 0.60. Overall, most spectral indices displayed significant correlations with LNC during the seedling establishment and flowering initiation stages ($p < 0.01$). However, in the maturation phase, although some indices maintained significance, such as the VARI with a correlation of 0.16, the overall correlation strength notably diminished.

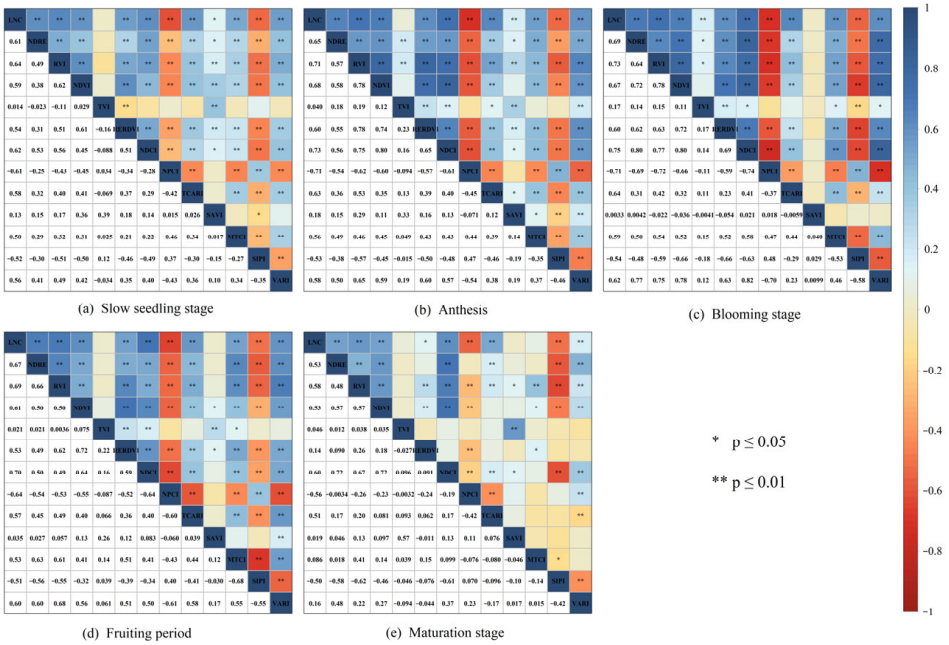

Figure 5. Correlation of spectral variables with measured LNCs.

To mitigate the risk of severe multicollinearity or overfitting among the vegetation indices used for modeling, the data from the full flowering period, which exhibited the highest correlation, were selected for further analysis. A stepwise multiple linear regression analysis was conducted using the SPSS 26.0 software on these variables, with variance inflation factors (VIFs) employed to detect multicollinearity among the vegetation indices. This approach effectively reduced the interference of redundant information while ensuring the independence of selected variables and the robustness of the model. The results, presented in Table 2, indicated that the VIF for the 10 input parameters was less than three, confirming the absence of multicollinearity among these vegetation indices. Consequently, the risk of overfitting was substantially reduced.

Table 2. Results of stepwise multiple linear regression analyses.

Input Variable	Beta	Tolerance	VIF
RVI	0.232	0.618	1.617
NDRE	0.060	0.451	2.217
NDVI	0.050	0.455	2.198
RERDVI	0.081	0.534	1.874
NDCI	0.191	0.510	1.959
NPCI	−0.219	0.606	1.649
TCARI	0.187	0.703	1.422
MTCI	0.136	0.731	1.368
SIPI	−0.067	0.620	1.613
VARI	0.075	0.646	1.548

3.3. Comparison of LNC Modeling Effectiveness of Processed Tomatoes in Different Fertility Periods

Based on the correlation analysis between the spectral variables and the LNC, it was observed that the correlation coefficients for TVI and SAVI across various growth stages were consistently below 0.20, indicating the lack of a significant relationship. Consequently, the following spectral-sensitive variables were selected for modeling: NDCI, NDRE, NPCI, RVI, NDVI, TCARI, VARI, RERDVI, MTCI, and SIPI. Notably, the NDCI exhibited the highest correlation during the flowering stage, reaching an impressive 0.75. In light of this finding, the NDCI was chosen as a singular variable, alongside the aforementioned ten sensitive spectral variables, to construct three distinct models—namely, BP, MLR, and RF. Each model was subjected to precision testing to ascertain the most optimal estimation model.

3.3.1. Construction of Estimation Models Using a Single Variable

The results of estimating the LNC using the NDCI index as a singular variable across different growth stages, as presented in Table 3 and Figures 6–8, indicate that, among the three estimation models, the RF model demonstrated the most optimal performance. Specifically, during the seedling and flowering initiation stages, the explanatory power of the NDCI was relatively limited, resulting in a decreased model stability and a constrained effectiveness in estimating LNC. In contrast, during the peak flowering stage, the NDCI exhibited its most significant predictive capability, with the RF model achieving an R^2 of 0.874, alongside low values for both the *RMSE* and *MAE*. This suggests that, during the peak flowering period, the physiological activities of the plants were at their zenith, enhancing the correlation between the NDCI and leaf nitrogen content, thereby yielding the most accurate predictions. However, as the plants transitioned into the fruit setting and maturation stages, there was a marked decline in the model's predictive performance. The R^2 values during the validation phase fell to 0.730 and 0.750, accompanied by a significant increase in both the *RMSE* and *MAE*. This decline in performance may be attributed to alterations in the plants' nitrogen requirements during these stages, as the growing fruits exerted a complex influence on the leaf nitrogen content, thereby complicating the predictive capabilities of the model.

Table 3. Results of LNC estimation by NDCI index at different fertility stages.

Growth Period	Model	Modeling			Validation		
		R^2	RMSE	MAE	R^2	RMSE	MAE
Slow seedling stage	RF	0.702	1.183	0.837	0.635	1.444	1.011
	BP	0.706	1.210	0.987	0.621	1.500	1.119
	MLR	0.629	1.290	1.026	0.588	1.459	1.166
Anthesis	RF	0.747	1.222	0.980	0.639	1.695	1.370
	BP	0.675	1.417	1.085	0.618	1.150	1.498
	MLR	0.701	1.662	1.359	0.595	1.519	1.434
Blooming stage	RF	0.706	0.986	0.691	0.874	0.663	0.503
	BP	0.710	1.140	1.022	0.732	1.136	0.946
	MLR	0.703	1.270	1.019	0.695	1.314	0.920
Fruiting period	RF	0.656	1.487	1.161	0.730	1.699	1.389
	BP	0.628	1.599	1.237	0.614	1.349	1.417
	MLR	0.651	1.618	1.171	0.608	1.757	1.656
Maturation stage	RF	0.746	1.494	1.184	0.750	1.891	1.521
	BP	0.702	1.393	1.174	0.709	1.904	1.563
	MLR	0.694	1.681	1.291	0.682	1.920	1.799

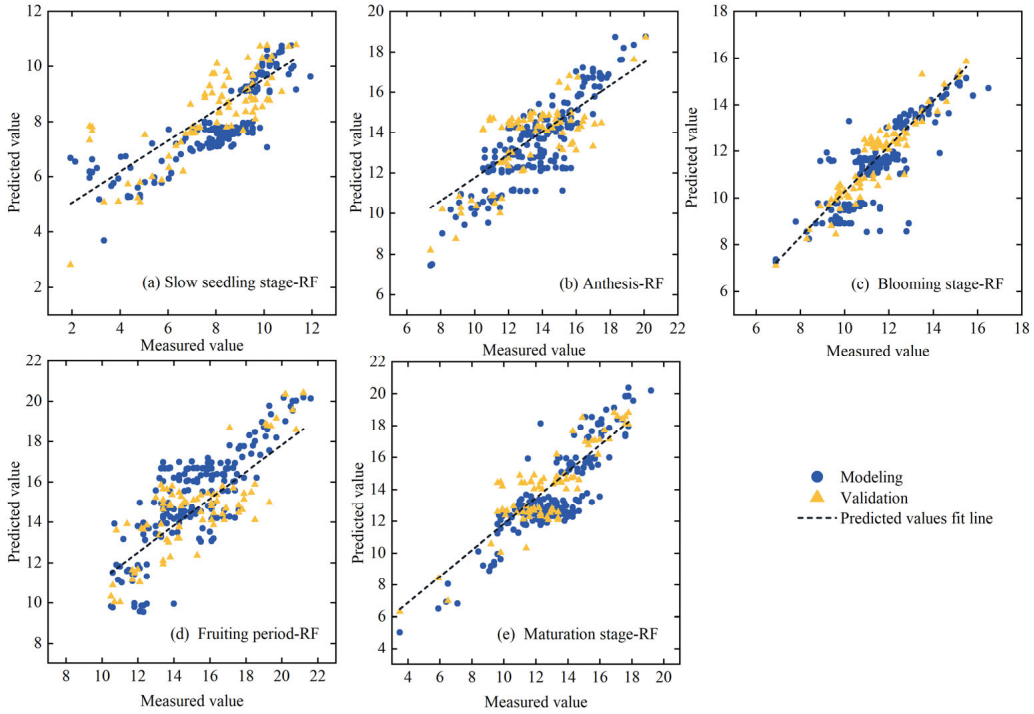

Figure 6. NDCI-based RF estimation of processed tomato LNC results.

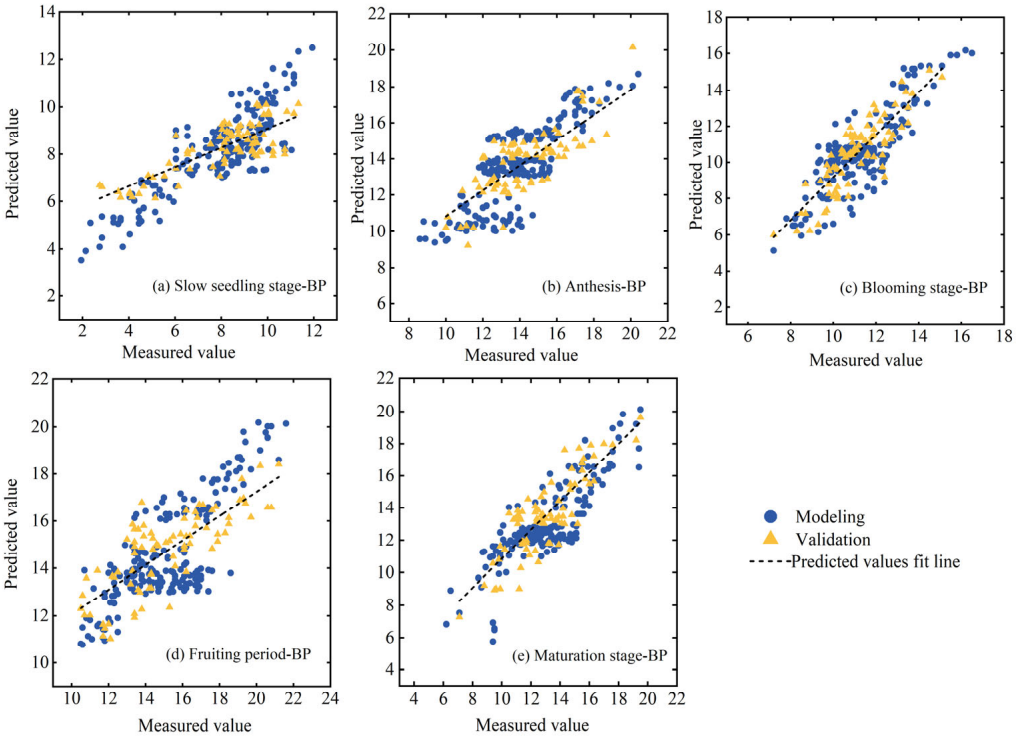

Figure 7. NDCI-based BP estimation of processed tomato LNC results.

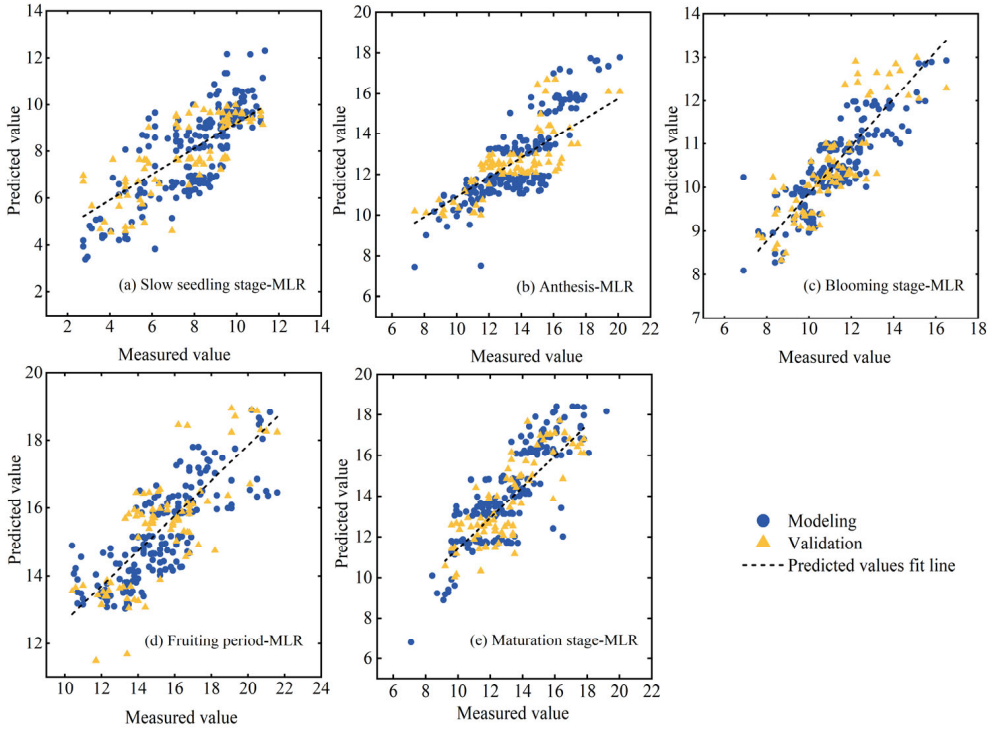

Figure 8. NDCI-based MLR estimation of processed tomato LNC results.

3.3.2. Construction of Estimation Models Using Multiple Variables

The results of estimating the LNC using various indices as variables across different growth stages are illustrated in Table 4 and Figures 9–11. During the seedling stage, the RF model demonstrated the most superior performance, with R^2 values of 0.824 for the training set and 0.825 for the validation set. In the flowering initiation stage, the RF model continued to exhibit commendable results, achieving R^2 values of 0.825 and 0.842 for the training and validation sets, respectively. In the peak flowering stage, the MLR model outperformed both the BP and RF models, attaining R^2 values of 0.875 and 0.865 for the training and validation sets, respectively. This phase was characterized by heightened photosynthetic activity and significant fluctuations in the LNC, allowing the MLR model to effectively capture the intricate relationships within the data. As the plants progressed into the fruit setting and maturation stages, the BP model emerged as the most effective, with R^2 values of 0.886 and 0.875 for the training set, as well as 0.810 and 0.827 for the validation set. Overall, it is evident that the performances of different models varied throughout the various growth periods, with the models established during the peak flowering and flowering initiation stages demonstrating the most robust predictive capabilities.

Table 4. Results of LNC estimation using 10 vegetation indices at different fertility stages.

Growth Period	Model	Modeling			Validation		
		R^2	RMSE	MAE	R^2	RMSE	MAE
Slow seedling stage	RF	0.824	0.652	0.426	0.825	0.996	0.823
	BP	0.732	0.956	0.799	0.823	0.998	0.812
	MLR	0.712	0.933	0.749	0.804	1.073	1.042
Anthesis	RF	0.825	0.728	0.553	0.842	0.983	0.820
	BP	0.717	1.036	0.868	0.803	1.107	0.936
	MLR	0.781	1.044	0.87	0.727	1.061	0.987
Blooming stage	RF	0.862	0.654	0.441	0.804	0.757	0.581
	BP	0.725	0.916	0.751	0.713	1.091	0.862
	MLR	0.875	0.561	0.575	0.865	0.732	0.653

Table 4. *Cont.*

Growth Period	Model	Modeling			Validation		
		R^2	RMSE	MAE	R^2	RMSE	MAE
Fruiting period	RF	0.883	0.991	0.705	0.792	1.192	0.994
	BP	0.886	0.850	0.698	0.810	1.111	0.924
	MLR	0.746	1.138	1.005	0.710	1.151	1.185
Maturation stage	RF	0.854	1.264	0.880	0.794	1.214	1.239
	BP	0.875	1.058	0.57	0.827	1.017	0.99
	MLR	0.733	1.254	1.11	0.671	1.057	1.219

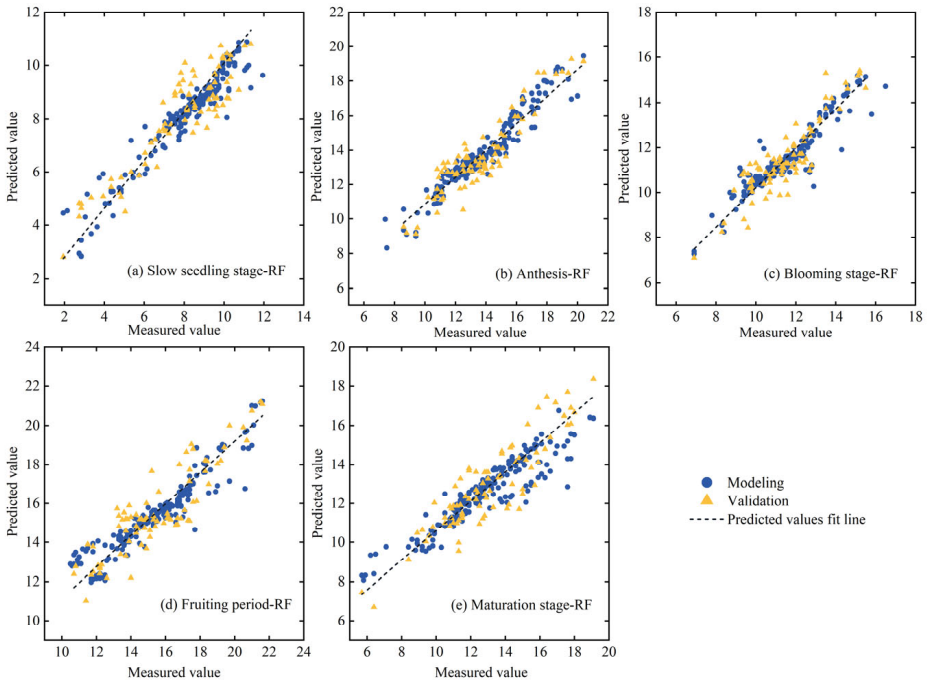

Figure 9. RF model estimation of processed tomato LNC results based on 10 vegetation indices.

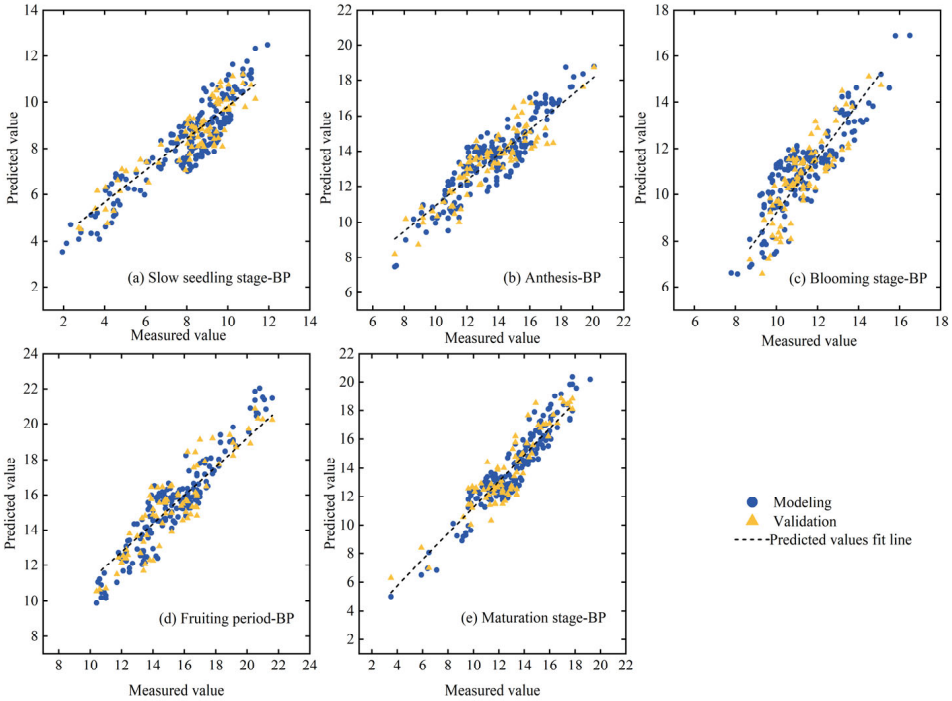

Figure 10. BP model estimation of processed tomato LNC results based on 10 vegetation indices.

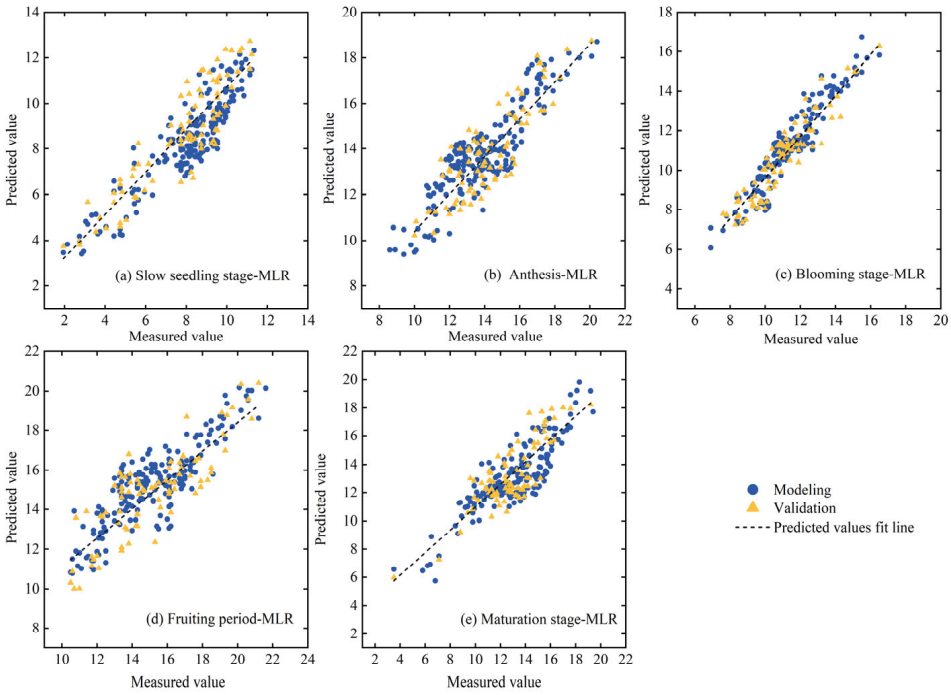

Figure 11. MLR model estimation of processed tomato LNC results based on 10 vegetation indices.

4. Discussion

The nitrogen requirements of processed tomatoes vary significantly across their five distinct growth stages, and this disparity directly influences their developmental processes. This relationship can be effectively reflected through the nitrogen content within their leaves [28,29]. Based on monitoring data from the past three years and previous studies [30], both unimodal and bimodal patterns have been observed in processed tomatoes. Generally speaking, a unimodal pattern indicates a concentrated supply of nutrients, while a bimodal pattern suggests the presence of two primary peaks of nutrient allocation during the growth period. This phenomenon was corroborated in the growth stages of processed tomatoes in Xinjiang, indicating that the demand for and distribution of nutrients change during different growth stages, potentially influenced by various factors such as climate, soil conditions, and management practices. Notably, during the peak flowering stage, nitrogen deficiency is most prevalent. This period not only necessitates nitrogen to facilitate the transition from large flower buds to fruit formation, but also requires adequate supplies to ensure the normal growth of the plant's stems and leaves [31]. Thus, the provision of nitrogen during this critical phase is essential for the growth and development of tomatoes.

This study evaluates the relationship between the spectral indices and LNC of processed tomato leaves across different growth stages. As processed tomato plants mature, the vegetation cover gradually increases [32]. The results reveal marked differences in the correlations between spectral indices and LNC at various growth stages. During the seedling and flowering initiation phases, when vegetation cover reaches 60%, several spectral indices (such as NDRE, RVI, and NDCI) exhibit a strong positive correlation with LNC, with correlation coefficients exceeding 0.6 ($p < 0.01$) [33]. Notably, both the RVI and NDVI show significant correlations with the leaf nitrogen content [34]. The effective absorption of nitrogen is crucial for plants during the early growth stages, and spectral indices can effectively reflect the physiological state of the vegetation. In the peak flowering stage, when vegetation cover reaches 60–80%, the NDCI demonstrates a significant positive correlation with leaf nitrogen content. During this phase, the crop's nitrogen demand markedly increases to support the development of floral organs, leading to a peak in leaf nitrogen content. This significant relationship indicates a close association between leaf ni-

trogen content and vegetation indices. However, in the fruit setting and maturation stages, when vegetation cover exceeds 80%, the correlation between spectral indices and LNC significantly declines. Particularly, the VARI (0.16) and RERDVI (0.14) during maturation exhibit notably low correlations. This decrease may be attributed to the oversaturation phenomenon that occurs as the cover transitions from below one to above one, resulting in a diminished variability or stagnation in certain vegetation indices [35]. When crops reach a certain growth threshold, limitations in soil nutrients or moisture may hinder further increases in vegetation indices [36]. Moreover, the focus of growth in processed tomatoes shifts towards fruit maturation, leading to the transfer of nitrogen from leaves to fruits. This transition results in a decrease in leaf nitrogen content, leaf senescence, chlorophyll degradation, and a reduction in photosynthetic capability, causing a less responsive reflection characteristic and further diminishing the variability of vegetation indices [37]. Additionally, it is observed that spectral indices such as SIPI and NPCI exhibit negative correlations in the later stages, which may reflect a reduced nitrogen use efficiency or growth inhibition due to an insufficient nitrogen supply [38,39].

By comparatively analyzing the performances of three models (RF, BP, and MLR) in modeling sets and validation sets with $R^2 \geq 0.8$ across different growth stages, several conclusions can be drawn. During the seedling and flowering initiation phases, the relatively small size of plant leaves and their limited photosynthetic capacity render remote sensing signals predominantly influenced by soil background [40,41]. The random forest (RF) model, by constructing multiple decision trees, effectively selects key features, mitigates data overfitting, and captures the influence of initial soil background values on vegetation spectral reflectance. Additionally, it adeptly models the nonlinear relationship between remote sensing signals and soil background. Its robustness and stability ensure that accurate and reliable predictions are maintained even under conditions of significant noise [42], making it particularly well-suited for analyzing remote sensing signals dominated by soil background during this stage. Moreover, while enhancing image resolution can more precisely capture subtle differences between plant leaves and the background, thereby reducing soil background interference, it also presents challenges related to an increased data volume and processing complexity. Therefore, a comprehensive consideration of both technological and resource aspects is essential to ensure the accuracy and practicality of data.

During the peak flowering stage, plant growth reaches its zenith, resulting in an enhanced linear relationship between growth parameters and remote sensing data. This allows multiple linear regression (MLR) to effectively capture variable correlations and improve prediction accuracy. Moreover, the remote sensing signals during this period are distinctly pronounced, characterized by a high vegetation cover and abundant chlorophyll content, which provide clear signals [43]. Additionally, stable environmental conditions reduce external noise interference, enabling MLR to more accurately capture the relationship between independent and dependent variables. This observation aligns with the findings of Meng et al. [44], who successfully monitored the leaf nitrogen content in tomatoes using the MLR model. Furthermore, during this stage, the random forest (RF) model, constructed using the normalized difference nitrogen index (NDCI), can swiftly monitor changes in leaf nitrogen content, corroborating the research conducted by Zhao et al. [45]. Thus, by employing these two methodologies, an effective assessment of the growth status and nutrient levels of processing tomatoes can be achieved during the peak flowering period. In the fruit setting and maturation stages, as plant fruits gradually ripen, the stems and leaves undergo a complex process of senescence and decay. The backpropagation (BP) model, with its robust nonlinear modeling capabilities, dynamic feature extraction, good adaptability, and resistance to interference, proves particularly suitable for this phase, consistent

with the study by Hu et al. [46]. The BP neural network effectively captures the nonlinear relationships among various factors throughout the plant growth process and utilizes a multilayer structure to extract and learn dynamic changes in features, maintaining a high predictive capability. Even amidst external disturbances, it adeptly adjusts to optimize the simulation and prediction of plant growth [47].

Moreover, the growth process of processed tomatoes is inherently complex, influenced by multiple factors such as variety, growth environment, and climatic conditions. A comprehensive consideration of these factors will enhance the monitoring efficacy of leaf nitrogen content. Future research could focus on several of the following key areas: (1) Data Acquisition: Employing hyperspectral data with a greater number of spectral bands can significantly enhance data accuracy, providing more precise information for monitoring the physiological state of crops. (2) Nutritional Element Monitoring: While this study centers on the monitoring of leaf nitrogen content in processed tomatoes, future investigations should aim to broaden the scope to include other essential nutrients such as phosphorus and potassium. This expansion would facilitate a more holistic view of the nutritional status of crops, thereby offering a scientific basis for the formulation of precise fertilization strategies. (3) Spatial Resolution and Remote Sensing Integration: By acquiring data at various spatial resolutions and integrating them with satellite remote sensing technology, it becomes possible to monitor crop growth and environmental conditions over a broader geographical area. This cross-scale monitoring capability not only aids in understanding the temporal and spatial dynamics of crop growth, but also provides critical data support for optimizing agricultural management practices and improving agricultural productivity. In summary, future research holds the promise of offering deeper and more comprehensive scientific guidance in the realms of crop management and agricultural sustainability.

5. Conclusions

This study employs multispectral imagery from unmanned aerial vehicles to monitor the LNC of processed tomatoes throughout various growth stages, leading to the following conclusions. During the entire growth cycle, the nitrogen content in the LNC of processed tomatoes exhibits pronounced phase-specific variations, characterized by a distinct bimodal pattern. In the early stages, the LNC is relatively low, demonstrating a strong positive correlation with multiple spectral indices such as NDRE, RVI, and NDCI. This indicates that nitrogen absorption during these phases is critical, with the plants exhibiting a substantial demand for nitrogen. As the growth stages advance, the LNC progressively increases, peaking during the fruit setting period, at which point the correlation between spectral indices and LNC significantly diminishes. This suggests that, during these later growth stages, the demand for nitrogen decreases, and the plants may increasingly rely on nutrients stored during the earlier phases. Through a comparative analysis of diverse monitoring models constructed from various vegetation indices over the entire growth period, it is evident that different methodologies can be employed at distinct growth stages for practical monitoring. When the vegetation coverage of processing tomatoes is between 60% and 80%, the RF monitoring model, based on the singular vegetation index, NDCI, can be effectively utilized for a rapid assessment of leaf nitrogen content. Conversely, when the vegetation coverage falls below 60% or exceeds 80%, a combined approach utilizing multiple vegetation indices and a multi-model comprehensive analysis is recommended. The most effective model should be selected as the primary tool, with additional models employed to validate results, thereby enhancing the reliability of predictions.

In the exploration of the integration between agricultural production and modern technology, selecting appropriate experimental subjects and environments is of paramount importance. However, this study also encounters several limiting factors that may affect

the generalizability and accuracy of the experimental results. Firstly, the processing tomato variety utilized in this experiment is Tunhe 1911. This specific cultivar exhibits unique growth characteristics, pest and disease resistance, and photosynthetic efficiency. However, it is crucial to note that different tomato varieties may respond significantly differently to environmental changes and technological applications. Consequently, the findings of this research may be confined to this particular variety and may not necessarily extend to other cultivars. Secondly, there may be limitations inherent in the spectral bands chosen for the UAVs employed in this study. As a vital tool in modern agricultural monitoring, the sensors and selected spectral bands carried by UAVs directly influence the efficacy of the monitoring process. In this study, the chosen spectral bands may not comprehensively cover the entire spectral range that could impact the growth of processed tomatoes, particularly in complex agricultural settings and under variable weather conditions, potentially leading to biases in the monitoring data. Moreover, the environmental differences across various regions represent another significant constraint of this research. This study was conducted in an arid to semi-arid climatic zone, where the unique climatic conditions may exert specific influences on the growth of processed tomatoes. This limitation restricts the applicability of the results to other climatic contexts, particularly in regions with abundant water resources or milder climates. In summary, these limiting factors serve as a reminder that when conducting agricultural technology experiments, it is essential to thoroughly consider the potential impacts of the selected subjects, technological choices, and environmental conditions on the experimental outcomes. This careful consideration is vital for enhancing the scientific rigor of the research and the applicability of its conclusions, ultimately fostering a more scientific, precise, and efficient approach to crop nutrient management.

Author Contributions: Conceptualization, H.Z. and H.W.; methodology, L.Z.; software, H.Z., X.M. and Y.S.; validation, H.Z. and H.W.; formal analysis, H.W. and L.Z.; investigation, M.J. and X.C.; resources, D.W.; data curation, H.Z. and M.J.; writing—original draft preparation, H.Z.; writing—review and editing, H.Z.; visualization, M.J.; supervision, H.W. and L.Z.; project administration, H.W. and D.W.; funding acquisition, H.W. All authors have read and agreed to the published version of the manuscript.

Funding: This study was supported by a grant from the project 'Ministry of Agriculture and Rural Affairs of China: Screening and Evaluation of Biodegradable Ground Film Products for Processing Tomatoes in Xinjiang' (Project No. 13230057).

Institutional Review Board Statement: Not applicable.

Data Availability Statement: The data presented in this study are available upon request from the corresponding author. The data are not publicly available due to their use in subsequent studies.

Conflicts of Interest: The authors declare no conflicts of interest.

References

1. Qian, X.; Wang, S.Y.; Wang, X.J.; Xue, J.L.; Bao, F.J. Effects of drip irrigation with CO, aqueous solution onagronomic traits and yield of processing tomato. *J. Zhejiang Agric. Sci.* **2024**, *65*, 1037–1041. [CrossRef]
2. Ronga, D.; Pentangelo, A.; Parisi, M. Optimizing N Fertilization to Improve Yield, Technological and Nutritional Quality of Tomato Grown in High Fertility Soil Conditions. *Plants* **2020**, *9*, 575. [CrossRef] [PubMed]
3. Soto, F.; Gallardo, M.; Thompson, R.B.; Peña-Fleitas, M.T.; Padilla, F.M. Consideration of total available N supply reduces N fertilizer requirement and potential for nitrate leaching loss in tomato production. *Agric. Ecosyst. Environ.* **2015**, *200*, 62–70. [CrossRef]
4. Zhang, F.; Liu, Y.; Liang, Y.; Dai, Z.; Zhao, Y.; Shi, Y.; Gao, J.; Hou, L.; Zhang, Y.; Ahammed, G.J. Improving the Yield and Quality of Tomato by Using Organic Fertilizer and Silicon Compared to Reducing Chemical Nitrogen Fertilization. *Agronomy* **2024**, *14*, 966. [CrossRef]

5. Yang, F.; Tian, J.; Meersmans, J.; Fang, H.; Yang, H.; Lou, Y.; Li, Z.; Liu, K.; Zhou, Y.; Blagodatskaya, E.; et al. Functional soil organic matter fractions in response to long-term fertilization in upland and paddy systems in South China. *CATENA* **2017**, *162*, 270–277. [CrossRef]
6. Zhang, K.; Wei, H.; Chai, Q.; Li, L.; Wang, Y.; Sun, J. Biological soil conditioner with reduced rates of chemical fertilization improves soil functionality and enhances rice production in vegetable-rice rotation. *Appl. Soil Ecol.* **2023**, *195*, 105242. [CrossRef]
7. Bustamante, S.C.; Hartz, T.K. Nitrogen Management in Organic Processing Tomato Production: Nitrogen Sufficiency Prediction Through Early-season Soil and Plant Monitoring. *HortScience* **2019**, *50*, 1055–1063. [CrossRef]
8. Lee, H.; Wang, J.; Leblon, B. Using Linear Regression, Random Forests, and Support Vector Machine with Unmanned Aerial Vehicle Multispectral Images to Predict Canopy Nitrogen Weight in Corn. *Remote Sens.* **2020**, *12*, 2071. [CrossRef]
9. Lu, N.; Wang, W.; Zhang, Q.; Li, D.; Yao, X.; Tian, Y.; Zhu, Y.; Cao, W.; Baret, F.; Liu, S.; et al. Estimation of Nitrogen Nutrition Status in Winter Wheat From Unmanned Aerial Vehicle Based Multi-Angular Multispectral Imagery. *Front. Plant Sci.* **2019**, *10*, 1601. [CrossRef]
10. Wang, S.W.; Niu, Y.X.; Ma, X.Y.; Chen, S.L.; Amani, N.; Feng, J. Prediction Model for Nitrogen Content of Rice Leaves during Heading Stage in Cold Region Based on Hyperspectrum. *J. Agric. Mech. Res.* **2019**, *41*, 158–164. [CrossRef]
11. Liu, H.; Zhu, H.; Wang, P. Quantitative modelling for leaf nitrogen content of winter wheat using UAV-based hyperspectral data. *Int. J. Remote Sens.* **2016**, *38*, 2117–2134. [CrossRef]
12. Li, Y.N. A tomato's Path to Industrialization. *People's Daily*, 23 September 2024; 010.
13. Shan, C.F.; Lan, Y.B.; Wang, J.; Liu, Q.; Zhao, D.; Lu, W.X. Method for Measuring Nitrogen Content in Crops and Precise Nitrogen Application. *J. Agric. Mech. Res.* **2021**, *43*, 146–150. [CrossRef]
14. Ranjan, R.; Chopra, U.K.; Sahoo, R.N.; Singh, A.K.; Pradhan, S. Assessment of plant nitrogen stress in wheat (*Triticum aestivum* L.) through hyperspectral indices. *Int. J. Remote Sens.* **2012**, *33*, 6342–6360. [CrossRef]
15. Rodriguez, D.; Fitzgerald, G.J.; Belford, R.; Christensen, L.K. Detection of nitrogen deficiency in wheat from spectral reflectance indices and basic crop eco-physiological concepts. *Aust. J. Agric. Res.* **2006**, *57*, 781–789. [CrossRef]
16. Verrelst, J.; Schaepman, M.E.; Koetz, B.; Kneubühler, M. Angular sensitivity analysis of vegetation indices derived from CHRIS/PROBA data. *Remote Sens. Environ.* **2008**, *112*, 2341–2353. [CrossRef]
17. Han, L.; Yang, G.; Dai, H.; Xu, B.; Yang, H.; Feng, H.; Li, Z.; Yang, X. Modeling maize above-ground biomass based on machine learning approaches using UAV remote-sensing data. *Plant Methods* **2019**, *15*, 10. [CrossRef]
18. Broge, N.H.; Leblanc, E. Comparing prediction power and stability of broadband and hyperspectral vegetation indices for estimation of green leaf area index and canopy chlorophyll density. *Remote Sens. Environ.* **2001**, *76*, 156–172. [CrossRef]
19. Fieuzal, R.; Marais Sicre, C.; Baup, F. Estimation of corn yield using multi-temporal optical and radar satellite data and artificial neural networks. *Int. J. Appl. Earth Obs. Geoinf.* **2016**, *57*, 14–23. [CrossRef]
20. Haboudane, D.; Miller, J.R.; Tremblay, N.; Zarco-Tejada, P.J.; Dextraze, L. Integrated narrow-band vegetation indices for prediction of crop chlorophyll content for application to precision agriculture. *Remote Sens. Environ.* **2002**, *81*, 416–426. [CrossRef]
21. Gitelson, A.A.; Kaufman, Y.J.; Stark, R.; Rundquist, D. Novel algorithms for remote estimation of vegetation fraction. *Remote Sens. Environ.* **2002**, *80*, 76–87. [CrossRef]
22. Gitelson, A.A.; Kaufman, Y.J.; Merzlyak, M.N. Use of a green channel in remote sensing of global vegetation from EOS-MODIS. *Remote Sens. Environ.* **1996**, *58*, 289–298. [CrossRef]
23. Huete, A.R. A soil-adjusted vegetation index (SAVI). *Remote Sens. Environ.* **1988**, *25*, 295–309. [CrossRef]
24. Dash, J.; Curran, P.J. The MERIS terrestrial chlorophyll index. *Int. J. Remote Sens.* **2004**, *25*, 5403–5413. [CrossRef]
25. Penuelas, J.; Filella, I.; Lloret, P.; Munoz, F.; Vilajeliu, M. Reflectance assessment of mite effects on apple trees. *Int. J. Remote Sens.* **1995**, *16*, 2727–2733. [CrossRef]
26. Yang, X.; Li, G.; Luo, W.; Chen, L.; Li, S.; Cao, M.; Zhang, X. Quantifying the Relationship between Leaf Nitrogen Content and Growth Dynamics and Yield of Muskmelon Grown in Plastic Greenhouse. *HortScience* **2015**, *50*, 1677–1687. [CrossRef]
27. Willmott, C.J.; Matsuura, K. Advantages of the mean absolute error (MAE) over the root mean square error (RMSE) in assessing average model performance. *Clim. Res.* **2005**, *30*, 79–82. [CrossRef]
28. Pourdarbani, R.; Sabzi, S.; Rohban, M.H.; García-Mateos, G.; Arribas, J.I. Nondestructive nitrogen content estimation in tomato plant leaves by Vis-NIR hyperspectral imaging and regression data models. *Appl. Opt.* **2021**, *60*, 9560–9569. [CrossRef]
29. Ulissi, V.; Antonucci, F.; Benincasa, P.; Farneselli, M.; Tosti, G.; Guiducci, M.; Tei, F.; Costa, C.; Pallottino, F.; Pari, L.; et al. Nitrogen Concentration Estimation in Tomato Leaves by VIS-NIR Non-Destructive Spectroscopy. *Sensors* **2011**, *11*, 6411. [CrossRef]
30. Tang, M.Y.; Zhang, Y.; Hu, G.Z.; Li, Q.J. Diagnostic Study of Nitrogen Fertilizer Use and Nitrogen Nutritional Status in Processing Tomatoes. *Soil Fertil. Sci. China* **2015**, *4*, 82–87.
31. Carrizo García, C.; Guarnieri, M.; Pacini, E. Soluble carbohydrates content in tomato pollen and its variations along and between blooming periods. *Sci. Hortic.* **2010**, *125*, 524–527. [CrossRef]
32. Zou, W.J.; Hua, S.; Xu, Z.F.; Xu, M.J.; Li, S.W.; Bao, W.N. Study on Estimation Method of Canopy Coverage for Facility Tomato Based on RGB Images. *North. Hortic.* **2024**, *3*, 41–50.

33. Li, H.; Li, D.; Xu, K.; Cao, W.; Jiang, X.; Ni, J. Monitoring of Nitrogen Indices in Wheat Leaves Based on the Integration of Spectral and Canopy Structure Information. *Agronomy* **2022**, *12*, 833. [CrossRef]
34. Oliveira, T.C.d.; Ferreira, E.; Dantas, A.A.A. Temporal variation of normalized difference vegetation index (NDVI) and calculation of the crop coefficient (Kc) from NDVI in areas cultivated with irrigated soybean. *Ciência Rural* **2016**, *46*, 1683–1688. [CrossRef]
35. Yanto, B.; Kartawidjaja, M.A.; Sukwadi, R.; Bachtiar, M. Implementation of hue saturation intensity (hsi) color space transformation algorithm with red, green, blue (rgb) color brightness in assessing tomato fruit maturity. *RJOCS Riau J. Comput. Sci.* **2023**, *9*, 167–178. [CrossRef]
36. Marino, S.; Alvino, A. Proximal sensing and vegetation indices for site-specific evaluation on an irrigated crop tomato. *Eur. J. Remote Sens.* **2014**, *47*, 271–283. [CrossRef]
37. Gamon, J.A.; Field, C.B.; Goulden, M.L.; Griffin, K.L.; Hartley, A.E.; Joel, G.; Penuelas, J.; Valentini, R.J. Relationships between NDVI, canopy structure, and photosynthesis in three Californian vegetation types. *Ecol. Appl.* **1995**, *5*, 28–41. [CrossRef]
38. Boussadia, O.; Steppe, K.; Van Labeke, M.C.; Lemeur, R.; Braham, M. Effects of Nitrogen Deficiency on Leaf Chlorophyll Fluorescence Parameters in Two Olive Tree Cultivars 'Meski' and 'Koroneiki'. *J. Plant Nutr.* **2015**, *38*, 2230–2246. [CrossRef]
39. Zeng, J.; Sheng, H.; Liu, Y.; Wang, Y.; Wang, Y.; Kang, H.; Fan, X.; Sha, L.; Yuan, S.; Zhou, Y. High Nitrogen Supply Induces Physiological Responsiveness to Long Photoperiod in Barley. *Front. Plant Sci.* **2017**, *8*, 569. [CrossRef]
40. Halliday, K.J.; Martínez-García, J.F.; Josse, E.-M. Integration of light and auxin signaling. *Cold Spring Harb. Perspect. Biol.* **2009**, *1*, a001586. [CrossRef]
41. Iglesias, M.J.; Sellaro, R.; Zurbriggen, M.D.; Casal, J.J. Multiple links between shade avoidance and auxin networks. *J. Exp. Bot.* **2017**, *69*, 213–228. [CrossRef]
42. Waske, B.; Heinzel, V.; Braun, M.; Menz, G. Random forests for classifying multi-temporal sar data. In Proceedings of the Proc.'Envisat Symposium, Montreux, Switzerland, 23–27 April 2007; pp. 23–27.
43. Zhou, Q.; Ismaeel, A. Integration of maximum crop response with machine learning regression model to timely estimate crop yield. *Geo-Spat. Inf. Sci.* **2021**, *24*, 474–483. [CrossRef]
44. Meng, L.; Zhang, J.; Yang, T.; Wu, L.-g. Study on the visual distribution of tomato leaf chlorophyll content based on hyperspectral imaging technology. *Hubei Agric. Sci.* **2022**, *61*, 171.
45. Zhao, R.-j.; Li, M.-z.; Yang, C.; Yang, W.; Sun, H. The canopy and leaf spectral characteristics and nutrition diagnosis of tomato in greenhouse. *Guang Pu Xue Yu Guang Pu Fen Xi = Guang Pu* **2010**, *30*, 3103–3106. [PubMed]
46. Hu, J.; Xin, P.; Zhang, S.; Zhang, H.; He, D. Model for tomato photosynthetic rate based on neural network with genetic algorithm. *Int. J. Agric. Biol. Eng.* **2019**, *12*, 179–185. [CrossRef]
47. Xing, H.H.; Lin, H.Y. An intelligent method optimizing BP neural network model. *Adv. Mater. Res.* **2013**, *605*, 2470–2474. [CrossRef]